ce/papers
The online collection for conference papers in civil engineering
Ernst & Sohn A Wiley Brand

ORIGINAL ARTICLE

SDSS 2022
The International Colloquium on Stability and Ductility of Steel Structures
14-16 September, University of Aveiro, Portugal
Ernst & Sohn A Wiley Brand

Structural Response of Wire Arc Additively Manufactured Steel Bolted Connections under Single Shear

Xi Guo[1], Pinelopi Kyvelou[1], Jun Ye[1], Lip H. Teh[2], Leroy Gardner[1]

Correspondence

Mr. Xi Guo
Department of Civil and Environmental Engineering
Imperial College London
Exhibition Road
SW7 2AZ London
Email: x.guo19@imperial.ac.uk

Abstract

An experimental investigation into the structural performance of wire arc additively manufactured (WAAM) steel single-lap shear bolted connections is presented in this paper. Sixty specimens of different thicknesses, printing strategies and geometric features, including end distances and plate widths, were manufactured using steel wire of a nominal yield strength of 420 MPa and subjected to single shear lap tests. The test results are analysed while the observed failure modes, featuring shear-out, net section tension fracture, end-splitting, localised tearing and curl-bearing failure, are discussed. Digital image correlation (DIC) was used for detailed monitoring and visualisation of the surface strain fields that developed during testing, providing valuable insight into the developed failure mechanisms. The experimental results, which generally followed the anticipated trends, were used to assess the applicability of current design specifications developed for conventional steel bolted connections to WAAM steel bolted connections. It was found that both the cold-formed steel specifications (AISI S100 and AS/NZS 4600) and the structural steel specifications (AISC 360 and EN 1993-1) yield considerable overestimations or underestimations of the test capacities, depending on the specimen geometry. Further research is underway to underpin the development of improved design provisions.

Keywords

3D printing, bolted connections, curl-bearing, end-splitting, localised tearing, shear-out, single-shear connections, tilt-bearing, wire arc additive manufacturing

1 Introduction

Wire arc additive manufacturing (WAAM) belongs to the directed energy deposition (DED) family of additive manufacturing methods and can be used to build large scale elements in an efficient manner [1-9]. The advantages of this innovative technology over conventional manufacturing methods, which include enhanced geometric versatility, increased automation and reduced material consumption [7,10], render WAAM capable of bringing about a step-change to the modus operandi of the construction industry. However, for this potential to be fully realised, a comprehensive understanding of the structural performance of WAAM steel members and connections is required.

Bolted connections are the most common type of connection used in steel construction, in which the load may be transmitted by means of shear in the bolts and bearing in the connected parts. Four distinct modes of failure were identified by Winter [11] for bolted connections: shear-out failure, bearing failure, net section tension failure and bolt shear failure – see Figure 1, with the latter type depending on the strength of the bolt (rather than that of the connected plates). Extensive research has been carried out thus far on bolted connections [12-31]. Several studies, particularly those featuring thin sheets under single shear, have revealed that the plates of lap connections can exhibit out-of-plane deformations, known as curling, resulting in reduced ultimate capacities [16,21,26].

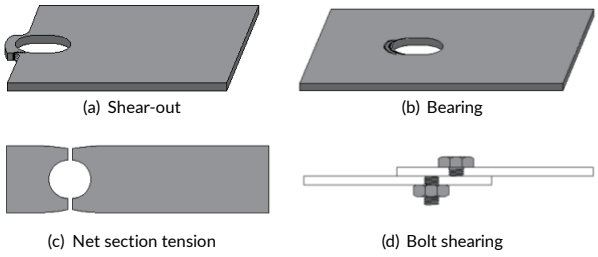

Figure 1 Conventional failrue modes for bolted connections

In this paper, the structural performance of WAAM steel bolted connections subjected to single shear is investigated. Sixty WAAM specimens of two different nominal thicknesses (3 mm and 8 mm) were manufactured with varying dimensions to obtain four distinct failure modes: net section tension fracture, shear-out, localised tearing and curl-bearing failure. The effects of material anisotropy and of the surface undulations inherent to the WAAM process on

[1] Department of Civil and Environmental Engineering, Imperial College London, London SW7 2AZ, UK
[2] School of Civil, Mining and Environmental Engineering, University of Wollongong, Wollongong 2500, Australia

the structural response of the examined connections were investigated by testing specimens with two different angles (0° and 90°) between the print layer orientation and the axis of loading. The particular geometric features of all specimens were captured by means of laser scanning, while digital image correlation (DIC) was employed to monitor the surface strain fields during testing. The observed failure modes are discussed herein and the applicability of current steel structural specifications [32-36] to the design of WAAM connections is assessed.

2 Manufacturing and geometric measurements

The test specimens were manufactured by MX3D [37], using their proprietary multi-axis robotic WAAM technology. Oval tubes of 3 mm and 8 mm nominal thickness were printed using EN ISO 14341-A: G 42 4 M21 3Si1 steel welding wire (equivalent to AWS A5.18: ER 70S-6). Test specimens were extracted from the flat sides of the tubes using a water jet cutter and were then sandblasted with glass beads to remove any welding soot from the WAAM process.

Sixty WAAM lap shear specimens of two different nominal thicknesses and two print layer orientations were fabricated, the basic configuration of which is shown in Figure 2, where d_0 is the bolt hole diameter, e_1 is the end distance between the centre of the bolt hole and the end of the WAAM plate, b is the plate width and x and y represent the directions perpendicular and parallel to the loading direction, respectively. The lengths of the specimens were approximately three times their respective widths, varying from 190 mm to 390 mm.

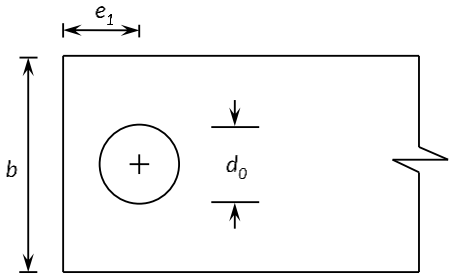

Figure 2 Basic geomtery of test specimens

The labelling for the test specimens begins with the letter S (for shear) followed immediately by the nominal thickness in mm, the nominal width b in mm, the end distance e_1 in mm and, finally, the angle in degrees between the axis of loading and the print layer orientation – see Figure 3. For example, Specimen S3-55-27-90 is a lap shear specimen with nominal values of thickness, width and end distance equal to 3 mm, 55 mm and 27 mm, respectively, with the axis of loading perpendicular to the print layer orientation.

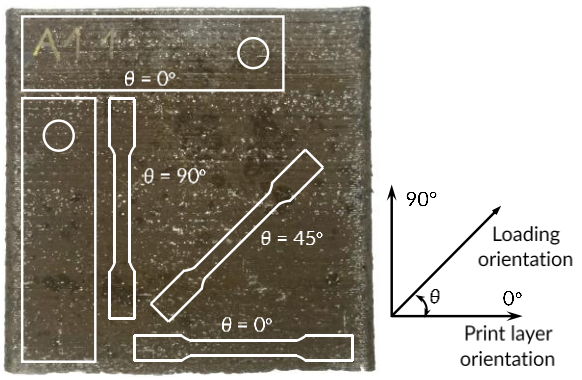

Figure 3 Orientation of tensile coupons and lap specimens extracted from WAAM plates relative to print layer orientation

The width b, end distance e_1 and bolt hole diameter d_0 of each test specimen were measured using Vernier callipers; the results are presented in Table 1. However, due to the inherent surface undulations of the as-built WAAM specimens, it has been shown that thickness measurements taken using conventional tools can be inaccurate [6,8]; 3D laser scanning was therefore employed. A FARO Design ScanArm 2.0, capable of recording 600,000 points per second with an accuracy of 0.075 mm [39], was used to obtain scans of both surfaces of each lap specimen, which were then merged into a single model represented as a point cloud in the software Geomagic Wrap [40]. The point cloud was subsequently inter-connected to form a polygonal mesh and a 3D CAD model, which was then imported into Rhino 3D [41] as an STL file to determine the average thickness of each specimen [6,8]. The values of the average thickness t of all specimens are given in Table 1.

Table 1 Measured geometric properties of test specimens

Specimen	Bolt type	t (mm)	d_0 (mm)	b (mm)	e_1 (mm)
S3-55-27-0	M16	2.7	18.0	55.1	26.9
S3-45-27-0	M16	3.0	17.8	45.4	27.3
S3-45-36-0	M16	3.0	17.7	45.4	36.3
S3-35-27-0	M16	2.7	17.9	34.8	26.8
S3-65-18-0	M16	2.8	17.8	65.5	18.2
S3-65-21.6-0	M16	2.9	17.8	65.4	21.6
S3-65-27-0	M16	2.9	17.8	65.3	27.0
S3-65-32.4-0	M16	2.8	17.8	65.4	32.5
S3-65-36-0	M16	2.8	17.8	65.5	36.3
S3-85-33-0	M20	2.8	21.8	85.5	33.3
S3-85-44-0	M20	2.7	21.7	85.4	44.3
S3-105-33-0	M20	2.6	22.2	105.0	32.9
S3-105-39.6-0	M20	2.6	22.6	105.0	39.3
S3-105-44-0	M20	2.7	22.2	105.1	44.1
S3-145-44.2-0	M24	2.7	26.2	144.0	43.8
S3-145-78-0	M24	2.7	26.3	143.4	78.2
S3-145-104-0	M24	2.6	26.3	144.2	104.2
S8-45-39-0	M24	7.3	26.4	45.1	38.9
S8-55-39-0	M24	7.5	26.2	55.0	39.1
S8-65-39-0	M24	7.5	26.2	64.7	39.1
S8-75-39-0	M24	7.6	25.9	75.0	39.0
S8-95-26-0	M24	7.5	25.9	95.1	26.1
S8-95-33.8-0	M24	7.6	26.1	95.3	33.9
S8-95-39-0	M24	7.5	25.9	95.3	39.2
S8-95-65-0	M24	7.4	25.9	94.9	65.0
S8-95-78-0	M24	7.4	25.9	94.9	78.3
S8-117-32-0	M30	7.4	32.0	117.2	32.1
S8-117-48-0	M30	7.6	31.7	117.1	47.8
S8-117-80-0	M30	7.5	31.8	117.3	79.9
S8-117-96-0	M30	7.6	31.9	117.3	96.0
S3-55-27-90	M16	2.7	18.1	54.5	26.8
S3-45-27-90	M16	2.9	17.9	45.5	27.4
S3-45-36-90	M16	2.9	17.8	45.3	36.3
S3-35-27-90	M16	2.7	18.1	34.8	26.9
S3-65-18-90	M16	3.0	17.8	65.5	18.3
S3-65-21.6-90	M16	2.9	17.8	65.3	21.8
S3-65-27-90	M16	2.9	17.7	65.3	27.0
S3-65-32.4-90	M16	2.9	17.8	65.3	32.4
S3-65-36-90	M16	2.9	17.8	65.1	36.3
S3-85-33-90	M20	2.8	21.9	85.6	33.4
S3-85-44-90	M20	2.8	21.9	85.6	44.4
S3-105-33-90	M20	2.8	22.2	105.1	33.0
S3-105-39.6-90	M20	2.8	22.1	105.1	39.0
S3-105-44-90	M20	2.8	22.1	104.9	43.6
S3-145-44.2-90	M24	2.7	25.9	144.0	40.8
S3-145-78-90	M24	2.7	26.2	145.1	78.1
S3-145-104-90	M24	2.7	26.2	143.9	103.4
S8-45-39-90	M24	7.4	26.2	44.7	38.8
S8-55-39-90	M24	7.5	26.2	54.9	38.9
S8-65-39-90	M24	7.3	26.2	64.9	39.2
S8-75-39-90	M24	7.5	26.2	75.2	38.9
S8-95-26-90	M24	7.7	25.9	95.2	26.1
S8-95-33.8-90	M24	7.6	26.0	95.2	34.0
S8-95-39-90	M24	7.7	25.9	95.0	39.2

S8-95-65-90	M24	7.7	25.8	95.1	65.1
S8-95-78-90	M24	7.6	25.9	94.9	78.2
S8-117-32-90	M30	7.5	32.0	117.2	32.2
S8-117-48-90	M30	7.5	31.9	117.2	48.3
S8-117-80-90	M30	7.6	31.9	117.2	80.2
S8-117-96-90	M30	7.6	32.0	117.2	96.2

3 Material tests

Twenty nine tensile coupon tests were conducted to determine the mechanical properties of the WAAM material. Anisotropy was investigated by testing coupons extracted from the WAAM plates at angles of 0° and 90° to the print layer orientation, as illustrated in Figure 3. Following their extraction from the parent plates using a water jet cutter, the coupons were sandblasted and laser scanned to obtain their average thickness and cross-sectional area.

The material tests were conducted in accordance with EN ISO 6892-1 [42], using a 250 kN Instron 8800 testing machine at a constant strain rate of 0.00007 s-1. A four-camera LaVision digital image correlation (DIC) system was employed to accurately monitor the surface strain fields on both sides of each coupon, over the parallel length. The acquired images, recorded at a frequency of 1 Hz, were processed in the software Davis [43].

A summary of the average material properties in each loading direction obtained from the coupon tests is presented in Table 2, where E is the Young's modulus, f_y is the yield strength defined as the 0.2% proof stress, f_u is the ultimate tensile strength, ε_u is the strain at f_u and ε_f is the fracture strain, determined over a standard gauge length of $5.65\sqrt{A}$, where A is the mean cross-section area along the parallel length [42]. The stress-strain curves for the 3 mm thick coupons are presented in Figure 4.

Table 2 Measured mechanical properties obtained from tensile coupon tests

t_{nom} (mm)	ϑ (°)	E (GPa)	f_y (MPa)	f_u (MPa)	ε_u	ε_f
3	0	208	394	500	0.15	0.19
	90	212	354	467	0.13	0.15
8	0	217	302	416	0.18	0.24
	90	198	282	409	0.16	0.20

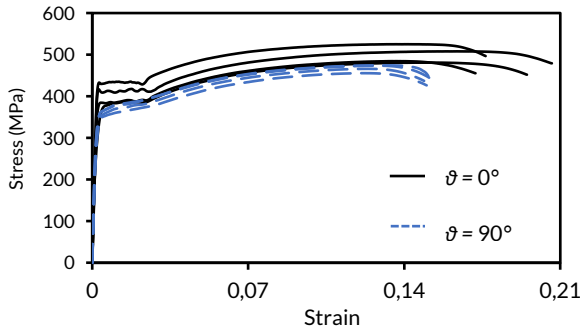

Figure 4 Stress-strain curves obtained from tensile coupon tests for 3mm thick coupons

The material anisotropy was found to be rather mild, with the variations in the Young's modulus, yield and ultimate tensile strengths due to material anisotropy all being within 10%. The strength of the thicker material was found to be consistently lower than the strength of the thinner material, with differences of up to 23% and 17% for the yield and ultimate tensile strengths, respectively; this is attributed to the slower cooling rate of the thicker material [44].

4 Lap shear connection tests

4.1 Test setup

An overview of the test setup employed for the lap shear tests is illustrated in Figure 5. Each test comprised a WAAM plate (i.e. the test specimen) connected to a conventional high strength steel (HSS) plate by means of a single fully threaded bolt in a 2 mm clearance bolt hole [29]. The bolt head and nut were finger-tightened to ensure contact at the interface of the plates, while limiting the influence of friction [45]. Note that the WAAM and HSS plates were of the same dimensions, ensuring the occurrence of failure within the (weaker) WAAM plate. The size (varying from M16 to M30) and grade (grade 12.9) of the bolts were selected such that shear failure of the bolts would be avoided.

All tests were conducted using a 600 kN Instron testing machine. The specimens were loaded using displacement control at a constant rate of 0.8 mm/min. A four-camera DIC system was employed to record the displacements and strain fields of both sides of the specimens, which were first painted black and then sprayed with a random white speckle pattern prior to testing to provide features for the DIC system to monitor – see Figure 5.

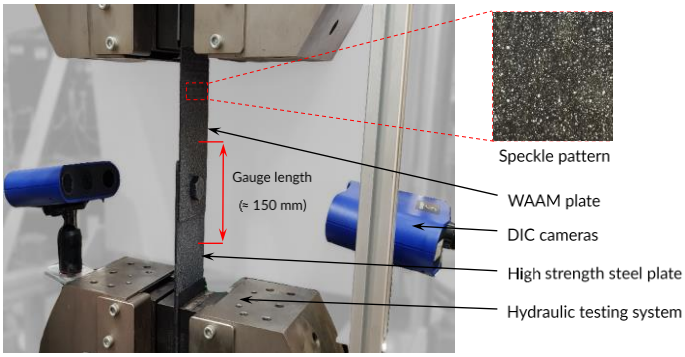

Figure 5 Experimental setup for lap shear connection tests

4.2 Failure modes

The observed failure modes of all tested specimens are reported in Table 3, where shear-out, net section tension, localised tearing, end-splitting and curl-bearing (see Section 4.2.3) failures are denoted by SO, NS, LT, ES and CB, respectively.

4.2.1 Shear-out, net section tension, end-splitting and bearing failures

As expected, shear-out failures developed in the specimens with short end distances e_1 and large plate widths b, while net section tension failures developed in the specimens with larger end distances e_1 and narrower plate widths b. End-splitting failure, on the other hand, which is characterised by in-plane bending and transverse tensile fracture at the specimen end, develops when the end distance e_1 is relatively short. It has been shown that the occurrence of either shear-out or end-splitting failure can be sensitive to the method used to cut the connected steel sheets [30,31]. It should be noted that pure bearing failures did not occur in the single-shear lap tests because of the tilting of the bolt and the curling of the plate. Instead, localised tearing or curl-bearing failures developed, when the end distance and the width of the plate were sufficiently large.

4.2.2 Localised tearing failure

The failure mode that is associated with fracture away from the minimum net section (i.e. at the centre of the bolt hole) combined with significant out-of-plane deformations is referred to as localised tearing. Localised tearing develops in elements made of ductile mild steel and can be viewed as a characteristic of localised bearing stress [16]. The evolution of tensile strain fields in typical cases of localised tearing failures is presented in Figure 6. In Figure 6(a), a butterfly shaped strain distribution can be observed at the later stages of loading, eventually leading to fracture at the bolt hole edge, as shown in Figure 6(b).

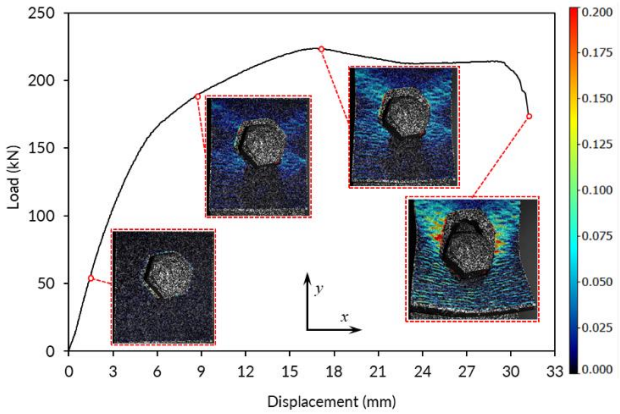

(a) Strain fields at different loading levels for the specimen

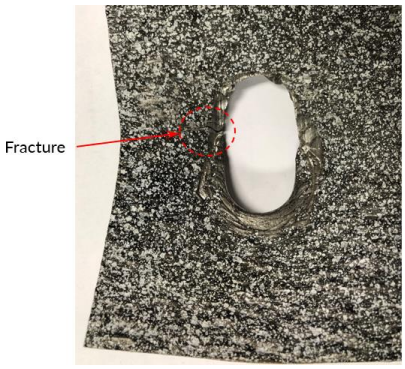

(b) Close-up view of the fracture

Figure 6 Specimen (S8-117-80-90) failing by localised tearing

4.2.3 Curling and curl-bearing failure

The out-of-plane deformation mode, known as curling (as distinct from curl-bearing failure, although this failure mode must be accompanied by curling), was observed for most specimens. As expected, curling was more pronounced in the thinner (i.e. 3 mm thick) plates. Although, in most cases, curling was not the direct cause of failure, in the tests of the thin plates where the end distances were extremely large, severe curling resulted in the bolt head penetrating into the lap plate downstream of the bolt hole – see Figure 7. This failure mode is referred to as curl-bearing failure in this paper, and to the authors' knowledge, has not been previously defined in the literature. In a sense, the curl-bearing failure mode is the "mirror" mode of the tilt-bearing failure mode identified by The and Uz [27], which involves the bolt head punching through the connected plate upstream as the bolt tilts backwards. Curl-bearing and tilt bearing failure modes therefore share a similar fracture mechanism.

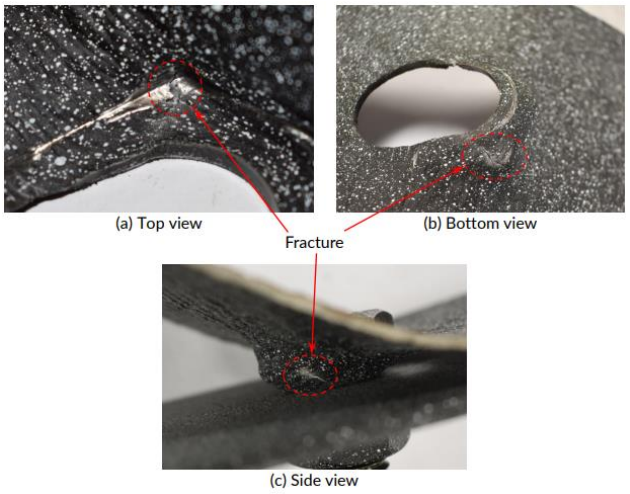

Figure 7 Close-up view of bolt head penetrating into plate – curl-bearing failure (Specimen S3-145-104-90)

4.3 Ultimate loads and load-deformation responses

The ultimate loads P_u attained by all specimens are summarised in Table 3. Note that the displacements (averaged from the two sides of the specimens) were measured over a gauge length of about 150 mm – see Figure 5. Typical load-displacement curves of specimens exhibiting shear-out and curl-bearing failures are presented in Figure 8. It can be observed that, while the curves corresponding to specimens failing by shear-out, net section tension and end-splitting have one distinct peak, the curves of specimens failing by localised tearing and curl-bearing have two peaks. This phenomenon is associated with the occurrence of curling, which, as observed during the tests, corresponded to the initial drop in load (i.e. the first peak). Once significant curling had developed, the resistance increased until the attainment of the second peak triggered by localised fracture.

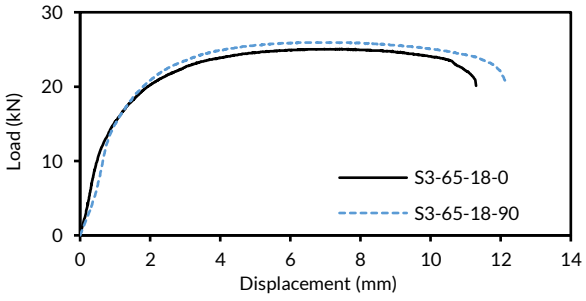

(a) Shear-out failure

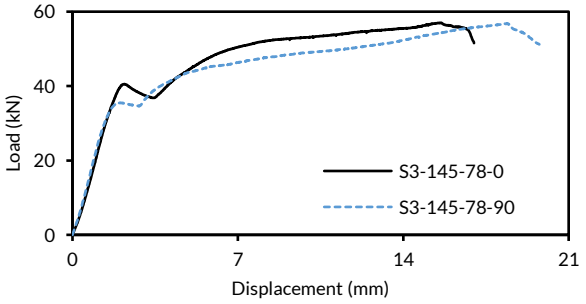

(b) Curl-bearing failure

Figure 8 Load-displacement curves of pairs of specimens with ϑ = 0° and ϑ = 90° exhibiting: (a) shear-out and (b) curl-bearing failure

Table 3 Summary of experimental results (FM = failure mode) and comparisons with design standards (SO: shear-out; NS: net section; B: bearing; LT: localised tearing; ES: end-splitting and CB: curl-bearing failure, in brackets if different from test results)

Specimen	Test			AISI S100		AISC 360		AS/NZS 4600		Eurocode 3	
	P_u (kN)	FM	Curling	$\frac{P_u}{P_{AISI}}$	FM	$\frac{P_u}{P_{AISC}}$	FM	$\frac{P_u}{P_{AS/NZS}}$	FM	$\frac{P_u}{P_{EC3}}$	FM
S3-35-27-90	21.44	NS		1.07	NS	1.01	NS	1.07	NS	1.01	NS
S3-35-27-0	21.53	NS		1.02	NS	0.96	NS	1.02	NS	0.96	NS
S3-45-27-90	35.51	NS+LT	✓	1.17	(SO)	0.94	NS	1.00	NS	1.06	(SO)
S3-45-27-0	37.13	NS+LT	✓	1.14	(SO)	0.91	(SO)	0.97	NS	1.02	(SO)
S3-45-36-90	36.12	NS+LT	✓	1.03	NS	0.96	NS	1.03	NS	0.96	NS
S3-45-36-0	37.17	NS+LT	✓	0.96	NS	0.90	NS	0.96	NS	0.90	NS
S3-55-27-90	36.30	LT	✓	1.38	(SO)	1.10	(SO)	1.09	(SO)	1.24	(SO)
S3-55-27-0	39.28	LT	✓	1.38	(SO)	1.10	(SO)	1.10	(SO)	1.24	(SO)
S3-65-18-90	25.97	SO		1.67	SO	1.34	SO	1.03	SO	1.15	SO
S3-65-18-0	25.08	SO		1.59	SO	1.27	SO	0.97	SO	1.08	SO
S3-65-21.6-90	31.12	SO		1.48	SO	1.19	SO	1.05	SO	1.17	SO
S3-65-21.6-0	31.70	SO		1.43	SO	1.15	SO	1.01	SO	1.13	SO
S3-65-27-90	43.95	LT	✓	1.49	(SO)	1.19	(SO)	1.20	(SO)	1.33	(SO)
S3-65-27-0	42.59	SO	✓	1.33	SO	1.07	SO	1.07	SO	1.19	SO
S3-65-32.4-90	44.30	LT	✓	1.15	(SO)	0.92	(SO)	1.00	(SO)	1.11	(SO)
S3-65-32.4-0	43.71	LT	✓	1.10	(SO)	0.88	(SO)	0.96	(SO)	1.07	(SO)
S3-65-36-90	42.50	LT	✓	0.96	(SO)	0.77	(SO)	0.88	(B)	0.97	(SO)
S3-65-36-0	43.10	LT	✓	0.92	(SO)	0.74	(SO)	0.84	(B)	0.93	(SO)
S3-85-33-90	42.78	LT	✓	1.24	(SO)	0.99	(SO)	1.00	(SO)	1.09	(SO)
S3-85-33-0	48.88	LT	✓	1.32	(SO)	1.05	(SO)	1.06	(SO)	1.16	(SO)
S3-85-44-90	49.41	LT	✓	0.96	(SO)	0.77	(SO)	0.87	(SO)	0.95	(SO)
S3-85-44-0	50.46	LT	✓	0.92	(SO)	0.73	(SO)	0.83	(SO)	0.90	(SO)
S3-105-33-90	47.54	LT	✓	1.41	(SO)	1.13	(SO)	1.12	(SO)	1.25	(SO)
S3-105-33-0	47.67	SO	✓	1.39	SO	1.11	SO	1.11	SO	1.22	SO
S3-105-39.6-90	53.21	LT	✓	1.20	(SO)	0.96	(SO)	1.03	(SO)	1.14	(SO)
S3-105-39.6-0	48.02	LT	✓	1.10	(SO)	0.88	(SO)	0.94	(SO)	1.06	(SO)
S3-105-44-90	50.88	LT	✓	0.99	(SO)	0.79	(SO)	0.89	(SO)	0.98	(SO)
S3-105-44-0	51.12	LT	✓	0.96	(SO)	0.77	(SO)	0.86	(SO)	0.95	(SO)
S3-145-44.2-90	46.30	LT	✓	1.10	(SO)	0.88	(SO)	0.90	(SO)	0.97	(SO)
S3-145-44.2-0	49.32	LT	✓	1.01	(SO)	0.81	(SO)	0.85	(SO)	0.92	(SO)
S3-145-78-90	56.81	CB	✓	0.83	(B)	0.62	(B)	0.83	(B)	0.63	(SO)
S3-145-78-0	57.03	CB	✓	0.77	(B)	0.58	(B)	0.77	(B)	0.59	(SO)
S3-145-104-90	55.88	CB	✓	0.83	(B)	0.62	(B)	0.83	(B)	0.62	(B)
S3-145-104-0	54.34	CB	✓	0.77	(B)	0.58	(B)	0.77	(B)	0.58	(B)
S8-45-39-90	62.71	NS		1.18	NS	1.12	NS	1.18	NS	1.12	NS
S8-45-39-0	60.44	NS		1.13	NS	1.07	NS	1.13	NS	1.07	NS
S8-55-39-90	95.75	NS		1.15	NS	1.08	NS	1.15	NS	1.08	NS
S8-55-39-0	101.11	NS		1.20	NS	1.13	NS	1.20	NS	1.13	NS
S8-65-39-90	118.77	NS		1.27	(SO)	1.03	NS	1.10	NS	1.11	(SO)
S8-65-39-0	123.78	NS		1.28	(SO)	1.03	NS	1.10	NS	1.11	(SO)
S8-75-39-90	133.38	ES		1.39	(SO)	1.12	(SO)	1.11	(SO)	1.21	(SO)
S8-75-39-0	146.77	ES+SO		1.49	SO	1.19	SO	1.19	SO	1.29	SO
S8-95-26-90	84.56	SO		1.70	SO	1.36	SO	1.03	SO	1.11	SO
S8-95-26-0	88.61	SO		1.79	SO	1.43	SO	1.08	SO	1.17	SO
S8-95-33.8-90	118.04	SO		1.51	SO	1.21	SO	1.12	SO	1.21	SO
S8-95-33.8-0	119.37	SO		1.51	SO	1.21	SO	1.12	SO	1.21	SO
S8-95-39-90	140.86	SO+ES		1.42	SO	1.13	SO	1.14	SO	1.23	SO
S8-95-39-0	135.59	SO+ES		1.38	SO	1.10	SO	1.11	SO	1.19	SO
S8-95-65-90	194.76	LT	✓	1.14	(B)	0.89	(NS)	1.14	(B)	1.02	(SO)
S8-95-65-0	174.51	LT	✓	1.05	(B)	0.82	(NS)	1.05	(B)	0.94	(SO)
S8-95-78-90	178.62	LT	✓	1.07	(B)	0.83	(NS)	1.07	(B)	0.83	(NS)
S8-95-78-0	191.19	LT	✓	1.14	(B)	0.89	(NS)	1.14	(B)	0.89	(NS)
S8-117-32-90	102.45	SO		1.73	SO	1.38	SO	1.04	SO	1.11	SO
S8-117-32-0	101.86	SO		1.70	SO	1.36	SO	1.02	SO	1.09	SO
S8-117-48-90	162.28	ES		1.35	(SO)	1.08	(SO)	1.09	(SO)	1.16	(SO)
S8-117-48-0	168.14	ES		1.39	(SO)	1.12	(SO)	1.12	(SO)	1.18	(SO)
S8-117-80-90	223.89	LT	✓	1.06	(B)	0.84	(NS)	1.06	(B)	0.95	(SO)
S8-117-80-0	210.80	LT	✓	1.00	(B)	0.79	(NS)	1.00	(B)	0.89	(SO)
S8-117-96-90	208.02	LT	✓	1.00	(B)	0.79	(NS)	1.00	(B)	0.79	(NS)
S8-117-96-0	213.78	LT	✓	1.00	(B)	0.79	(NS)	1.00	(B)	0.79	(NS)
Mean				1.22		0.99		1.02		1.04	
COV				0.21		0.22		0.11		0.17	

4.4 Influence of print orientation

The angle ϑ between the axis of loading and the print layer orientation was not found to have a significant influence on neither the load-desplacement responses nor the failure modes of most specimens due to the rather mild anisotropy. However, some specimens of the same nominal dimensions but of different print layer orientations (i.e. ϑ = 0° and 90°), failed in different modes and fractured at different locations. This is attributed to the fracture lines developing along the interface of adjoining print layers.

5. Comparisons between the test results and existing design equations

The resistances of the examined specimens, as determined by physical testing, are compared against the strength predictions given by the design equations set out in current steel design standards, namely AISI S100 [32], AISC 360 [33], Eurocode 3 [34, 35] and AS/NZS 4600 [36], to assess their suitability for application to WAAM lap shear connections. The strength predictions used for the comparisons presented herein were derived using the measured geometric and material properties and the results of the comparison are presented in Table 3.

Among the current steel design standards, the most accurate capacity predictions were yielded by AS/NZS 4600 [36], with an average test-to-predicted capacity ratio of 1.02 in conjunction with a coefficient of variation (COV) of 0.11 – see Table 7. Although the equations of AISC 360 [33] led to an average capacity ratio of 0.99, the resulting COV was double that of the AS/NZS 4600 equations. Overall, the AISI S100 equations [32] were found to be the most conservative as they underestimated the capacity of the WAAM connections by 22% on average, with a COV of 0.21. Eurocode 3 [34, 35] is also conservative, with an average test-to-predicted capacity ratio of 1.04 and a COV of 0.17. The comparison of the experiment results for shear-out and bearing failure as well as for bearing and net section tension failure, are presented in Figures 9 and 10 respectively.

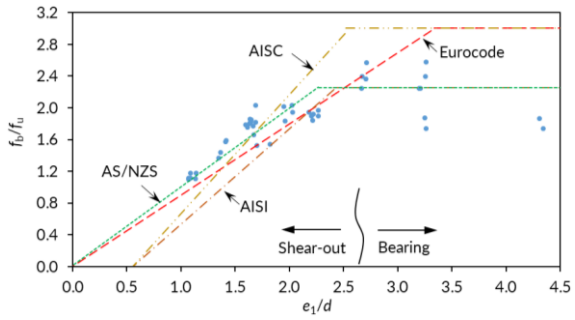

Figure 9 Comparison of experimental results and design equations for shear-out and bearing, where shear-out and bearing failure, as described by the considered design codes, are indicated

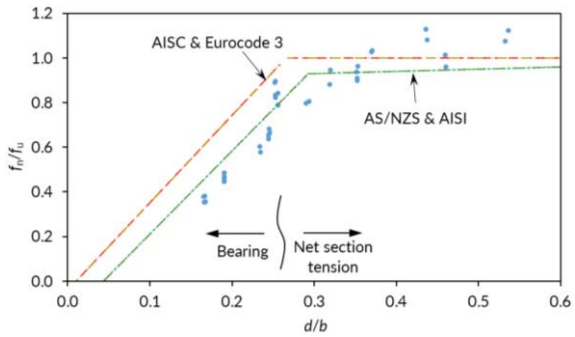

Figure 10 Comparison of experimental results and design equations for bearing and net section tension, where net section tension and bearing failure, as described by the considered design codes, are indicated

6. Conclusion

A total of 60 WAAM steel single-lap shear bolted connections of two different nominal thicknesses, two different print layer orientations and varying dimensions were tested. The measured material properties, geometries, load-deformation characteristics and failure modes (including shear-out, localised tearing, curl-bearing and net section tension fracture) of the test specimens are reported and analysed. The ultimate test loads were compared against the predictions of four major design standards for either structural/hot-rolled (AISC 360 and EN 1993-1-8) or cold-formed (AISI S100 and AS/NZS 4600) steel.

The experimental programme revealed that the print layer orientation has little influence on the deformation and load-carrying capacities of the WAAM connections. Although, in some cases, the failure mode was found to be dependent on the print layer orientation, the ultimate test loads were essentially unaffected, showing that the same structural design equations can be used for different print layer orientations.

Specimens with sufficiently large end distances (to avoid shear-out failure) and widths (to avoid net section tension fracture) failed predominantly in localised tearing. However, specimens with larger end distances experienced severe curling, resulting in the bolt head punching through the connected plate downstream, as the bolt moves in the loading direction. This failure mode is defined as curl-bearing failure in the present paper.

Overall, although the WAAM test specimens exhibited the anticipated trends, their failure loads were generally well predicted by the existing design standards, with AS/NZS 4600 providing the most accurate capacity predictions. Further research is required to assess reliability and to derive suitable safety factors for use in the design of WAAM connections.

References

[1] L. Gardner, P. Kyvelou, G. Herbert, C. Buchanan, Testing and initial verification of the world's first metal 3D printed bridge. J. Construct. Steel Res. 172 (2020) 106233.

[2] N. Hadjipantelis, B. Weber, C. Buchanan, L. Gardner, Description of anisotropic material response of wire and arc additively manufactured thin-walled stainless steel elements, Thin-Walled Struct. 171 (2022) 108634.

[3] V. Laghi, M. Palermo, L. Tonelli, G. Gasparini, L. Ceschini, T. Trombetti, Tensile properties and microstructural features of 304L austenitic stainless steel produced by wire and arc additive manufacturing. Int. J. Adv. Manuf. Technol. 106 (2020) 3693-3705.

[4] V.A. Silvestru, I. Ariza, J. Vienne, L. Michel, A.M. Aguilar Sanchez, U. Angst, R. Rust, F. Gramazio, M. Kohler, A. Taras, Performance under tensile loading of point-by-point wire and arc additively manufactured steel bars for structural components. Mater. Des 205 (2021) 109740.

[5] F. Martina, J. Mehnen, S.W. Williams, P. Colegrove, F. Wang, Investigation of the benefits of plasma deposition for the additive layer manufacture of Ti–6Al–4V, J. Mater. Process. Tech. 212 (6) (2012) 1377–1386.

[6] P. Kyvelou, C. Huang, L. Gardner, C. Buchanan, Structural testing and design of wire arc additively manufactured square hollow sections, J. Struct. Eng. 147 (2021) 1-19.

[7] C. Buchanan, L. Gardner, Metal 3D printing in construction: A review of methods, research, applications, opportunities and challenges, Eng. Struct. 180 (2019) 332–348.

[8] P. Kyvelou, H. Slack, D.D. Mountanou, M.A. Wadee, T.B. Britton, C. Buchanan, L. Gardner, Mechanical and microstructural testing of wire and arc additively manufactured sheet material, Mater. Des. 192 (2020) 108675.

[9] A. Kanyilmaz, A.G. Demir, M. Chierici, F. Berto, L. Gardner, S.Y. Kandukuri, P. Kassabian, T. Kinoshita, A. Laurenti, I. Paoletti, A. du Plessis, S.M.J. Razavi, Role of metal 3D printing to increase quality and resource-efficiency in the construction sector, Addit. Manuf. 50 (2022) 102541.

[10] J. Ye, P. Kyvelou, F. Gilardi, H. Lu, M. Gilbert, L. Gardner, An end-to-end framework for the additive manufacture of optimized tubular structures, IEEE Access 9 (2021) 165476-165489.

[11] G. Winter, Tests on bolted connections in light gage steel, J. Struct. Div. 82 (2) (1956) 1–25.

[12] R.A. Laboube, Strength of bolted connections: is it bearing or net section?, in: 9th Int. Specialty Conf. on Cold-Formed Steel Struct. (1988) 589–601.

[13] F. Zadanfarrokh, E.R. Bryan, Testing and design of bolted connections in cold formed steel sections, in: 11th Int. Specialty Conf. on Cold-Formed Steel Struct. (1992) 625–662.

[14] C.A. Rogers, G.J. Hancock, Bolted connection tests of thin G550 and G300 sheet steels, J. Struct. Eng. 125 (2) (1998) 128–136.

[15] C.A. Rogers, G.J. Hancock, Bolted connection design for sheet steels less than 1.0 mm thick, J. Constr. Steel Res. 51 (2) (1999) 123–146.

[16] C.A. Rogers, G.J. Hancock, Failure modes of bolted-sheet-steel connections loaded in shear, J. Struct. Eng. 126 (3) (2000) 288–296.

[17] J.A. Wallace, R.M. Schuster, Testing of bolted cold-formed steel connections in bearing (with and without washers), in: 16th Int. Specialty Conf. on Cold-Formed Steel Struct. (2002) 730–747.

[18] R. Puthli, O. Fleischer, Investigations on bolted connections for high strength steel members, J. Constr. Steel Res. 57 (3) (2001) 313–326.

[19] P. Može, D. Beg, High strength steel tension splices with one or two bolts, J. Constr. Steel Res. 66 (8–9) (2010) 1000–1010.

[20] Y. Wang, Y. Lyu, G. Li, Experimental investigation of two-bolt connections for high strength steel members, in: 12th Int. Conf. on Advances in Steel-Concrete Composite (2018) 595–600.

[21] T.S. Kim, H. Kuwamura, Finite element modeling of bolted connections in thin-walled stainless steel plates under static shear, Thin-Walled Struct. 45 (4) (2007) 407–421.

[22] E.L. Salih, L. Gardner, D.A. Nethercot, Numerical investigation of net section failure in stainless steel bolted connections, J. Constr. Steel Res. 66 (12) (2010) 1455–1466.

[23] E.L. Salih, L. Gardner, D.A. Nethercot, Bearing failure in stainless steel bolted connections, Eng. Struct. 33 (2011) 549–562.

[24] J.S. Lim, T.S. Kim, S.H. Kim, Ultimate strength of single shear bolted connections with cold-formed ferritic stainless steel, J. Zhejiang Univ. Sci. A (Appl. Phys. & Eng.) 14 (2) (2013) 120–136.

[25] Z.Wong, Y. Wang, X. Yun, L. Gardner, L.H. Teh, Experimental study of swage-locking pinned aluminium alloy shear connections, Thin-Walled Struct. 163(2021) 107641

[26] T.S. Kim, H. Kuwamura, T.J. Cho, A parametric study on ultimate strength of single shear bolted connections with curling, Thin-Walled Struct. 46 (2008) 38–53.

[27] L.H. Teh, M.E. Uz, Ultimate Tilt-Bearing Capacity of Bolted Connections in Cold-Reduced Steel Sheets, J. Struct. Eng. 143 (4) (2017) 04016206.

[28] L.H. Teh, M.E. Uz, Ultimate Shear-Out Capacities of Structural-Steel Bolted Connections, J. Struct. Eng. vol. 141(6) (2015) 04014152.

[29] L.H. Teh and B.P. Gilbert, Net Section Tension Capacity of Bolted Connections in Cold-Reduced Steel Sheets, J. Struct. Eng. 138 (3) (2012) 337–344.

[30] H. Xing, L.H. Teh, Z. Jiang, A. Ahmed, Shear-Out Capacity of Bolted Connections in Cold-Reduced Steel Sheets, J. Struct. Eng. 146(4) (2020) 04020018.

[31] C.O. Rex, W.S. Easterling, Behavior and Modeling of a Bolt Bearing on a Single Plate, J. Struct. Eng. 129 (6) (2003) 792–800.

[32] AISI, North American specification for the design of cold-formed steel structural members, AISI S100-16w/S1-18, Washington DC, American Iron and Steel Institue, 2016.

[33] AISC, Specification for structural steel buildings, ANSI/AISC 360-16, Chicago, American Institute of Steel Construction, 2016.

[34] Eurocode 3: design of steel structures – part 1-8: design of joints, prEN 1993-1-8, Brussels, European Committee for Standardisation, 2021.

[35] Eurocode 3: design of steel structures – part 1-1: general rules and rules for builidng, prEN 1993-1-1, Brussels, European Committee for Standardisation, 2020.

[36] AS/NZS, Cold-formed steel structures, AS/NZS 4600:2018, Sydney, Australian/New Zealand Standard, 2018.

[37] MX3D, About – MX3D, [online] Available from https://mx3d.com, accessed Mar. 15, 2021.

[38] EN ISO 14341: 2020 Welding consumables – Wire electrodes and weld deposits for gas shielded metal arc welding of non alloy and fine grain steels- Classification, International Organization for Standardization.

[39] FARO Design ScanArm 2.0 ®, 2018.

[40] 3D Systems, Geomagic Wrap 2017 (Version 2017.0.2:64) [Software] 2017 3D Systems, Incorporated and its licensors, 2017.

[41] Rhino 3D, Rhino 3D computer-aided design software (Version 5 SR14 64-bit) [Software] Robert McNeel & Associates, 2017.

[42] EN ISO 6892-1: 2019 Meallic materials – tensile testing, part1: Method of test at room temperature, International Organization for Standardization.

[43] LaVision, DaVis (Version 8.4.0) [Software] La Vision GmbH, 2017.

[44] C. Huang, P. Kyvelou, R. Zhang, T. B. Britton, L. Gardner, Mechanical testing and microstructure of wire arc additively manufactured steels, Mater. Des. 216 (2021) 110544.

[45] A. Talja, M. Torkar, Lap shear tests of bolted and screwed ferritic stainless steel connections, Thin-Walled Struct. 83 (2014) 157–168.